Quench analysis of large superconducting magnets. Part I: model description

L. Bottura and O.C. Zienkiewicz*

The NET Team, c/o Max Planck IPP, Boltzmannst. 2, D-8046 Garching, FRG
*Institute for Numerical Methods in Engineering, University College of Swansea, Swansea SA2 8PP, UK

Received 26 September 1991; revised 13 January 1992

In large superconducting magnets built using force-flow cooled conductors, such as those being designed for next generation fusion machines, the quench propagation is a three-dimensional phenomenon. In this paper we develop a method for the analysis of quenches in 3-D which is extremely versatile and comprehensive. The method is based on the parallel solution of a set of 1-D problems represented by the helium flow, heat conduction and quench propagation along the conductor length. Transverse heat exchange among conductors is then explicitly inserted in the model, thus achieving the desired 3-D capability. In the model developed for the 1-D analysis we have foreseen the possibility of taking into account the thermal gradients in the cable cross-section, and the changes of magnetic field and operating current which are typical of a quench transient.

Keywords: quench, protection, force-flow superconductors

The analysis of quench propagation for force-flow cooled conductors has always been a matter of fundamental importance for the design of the protection scheme of a superconducting magnet[1]. This is even more true for the large magnets which are under design for fusion machines of the next generation[2]. These magnets will be a considerable investment compared to the cost of the whole plant, and will store an amount of energy in the order of several tens of GJ. Therefore there is an increasing interest in the issues of safety and protection of these systems.

The quench propagation in force-flow cooled superconducting magnets has so far been studied only in a one dimensional (1-D) approximation, assuming that the dominating mode of propagation is that in the longitudinal direction of the cable (along the helium flow). This hypothesis is at the basis of most of the quench analysis codes developed in the last 15 years[3-7].

The one dimensional behaviour is only a simplifying assumption, and should be avoided if a more powerful modelling tool is available. In a real superconducting magnet, the initiation and the propagation of a normal zone depend not only on the longitudinal heat fluxes, but also on the heat diffusion in the winding pack cross-section, i.e. transverse to the main conductor axis. A normal zone can be initiated by heat conduction in turns or pancakes adjacent to the one initially quenched, thus increasing the normal zone propagation speed in the coil and decreasing the thermal gradients among neighbouring conductors. Therefore, one can expect that the calculations of the quench propagation and of the hot-spot temperature performed with the 1-D models are generally conservative, as in this approximation the energy deposition tends to be concentrated in the cable region initially quenched. For the cable design this means over-dimensioning the stabilizer and therefore losing efficiency. Furthermore, in the case of uncontrolled transients, the calculation performed in the 1-D approximation may predict catastrophic events that are not realistic, such as the loss of insulation or melting of the cable. The question of the relevance of the 1-D assumption is therefore not only of academic interest, and there is scope in changing this commonly used model to include 3-D effects in the calculation.

Finally, most of the 1-D approaches were based on approximate expressions for the Joule heating term in the superconducting strand, simplified functional dependence of the magnetic field on the conductor and of the time dependence of the operating current. Because we were starting the development of a new model, we decided to maintain it as general as possible, so that we would be able to cope with the large number of different situations arising in the design of a fusion magnet.

0011 – 2275/92/070659 – 09

The model presented here is based on a general cable configuration formed by the parallel channels of the helium flow and several longitudinal heat and current conductors, allowing for thermal gradients in the cable cross-section. It includes the 3-D effects by permitting the heat transfer between adjacent cables. This extension has been achieved in a simple manner preserving the transparency of the basic 1-D model. Current, magnetic field and source terms (e.g. Joule heating) are arbitrary. Finite elements are used in preference to finite differences as a way to increase accuracy and flexibility.

Basic equations

For a force-flow cooled conductor the helium flow can be regarded as 1-D along the cooling channels with a good degree of approximation. We assume throughout this work that the flow always remains in single phase, a condition satisfied when supercritical helium is used as coolant. The analysis of the quench propagation requires the solution of the following equations.

Fluid flow and energy transport equations for a 1-D channel

$$\frac{\partial \rho}{\partial t} + \frac{\partial (\rho v)}{\partial x} = 0 \tag{1}$$

$$\frac{\partial (\rho v)}{\partial t} + \frac{\partial (\rho v^2)}{\partial x} + \frac{\partial p}{\partial x} = 2f \frac{\rho v |v|}{D_h} \tag{2}$$

$$\frac{\partial (\rho e)}{\partial t} + \frac{\partial (\rho e v)}{\partial x} + \frac{\partial (pv)}{\partial x} = h \frac{S}{A_{he}} (T_s - T_{he}) \tag{3}$$

$$e = i + \frac{v^2}{2} \tag{4}$$

The set of unknowns is the density ρ, the velocity v, the helium pressure p and temperature T_{he}, the total and internal energy e and i respectively. In the above A_{he} is the cross-sectional area of the helium conduit, D_h is its hydraulic diameter and S is the perimeter of the surface on which the convective heat transfer from the solid takes place at temperature T_s. The two coefficients f and h are the friction factor and the heat transfer coefficients, descriptive of the turbulent flow conditions. A state equation is needed to relate pressure and temperature to internal energy i and density ρ.

Heat conduction in the solid composite

In the general case, the following form of the conduction equation in three dimensions holds:

$$\rho C \frac{\partial T_s}{\partial t} - \nabla (K \nabla T_s) = \dot{Q}_{ext} + \dot{Q}_J \tag{5}$$

with the following convective boundary condition for the heat flux on the surface S at the interface with the helium:

$$-K \frac{\partial T_s}{\partial n} \bigg|_S = h(T_s - T_{he}) \tag{6}$$

Here the unknown is the temperature of the solid, T_s. The properties of the solid materials to be specified are the heat capacity C and thermal conductivity K. The source terms are the external heating power density $\dot{Q}_{ext}$ and the Joule heating power density $\dot{Q}_J$. Finally, n represents the direction normal to the boundary, pointing outwards.

For the present purpose it is convenient to deal only with the 1-D form of the Equation (5) combined with the boundary condition (6), written along the longitudinal conductor axis x, valid for the hypothesis of an homogeneous conductor component i with cross-section A_i, heat capacity C_i, thermal conductivity K_i and temperature T_i.

$$A_i \rho C_i \frac{\partial T_i}{\partial t} - A_i \frac{\partial}{\partial x} \left(K_i \frac{\partial T_i}{\partial x} \right) =$$

$$h_1 S_{i-he} (T_{he} - T_i) + \sum_j h_{ij} S_{ij} (T_j - T_i) + A_i \dot{Q}_i \tag{7}$$

The source terms on the r.h.s. of Equation (7) are respectively the heat exchange with the helium at temperature T_{he} through a heat exchange coefficient h_1 and a contact surface S_{i-he}, heat exchange with another conductor j at temperature T_j through a heat exchange coefficient h_{ij} and a contact surface S_{ij}, and the density of heating power $\dot{Q}_i$ (external or Joule) per unit length.

Joule heat generation

Special attention in the superconducting composite is given to the Joule heat generation term. With reference to an electric conductor with negligible dimensions in transverse direction to the current flow, the Joule heating power is a function

$$\dot{Q}_J = \dot{Q}_J(T, B, J) \tag{8}$$

of the temperature T and the field B, in turn functions of position and time, and of the operating current density J in the conductor, dependent only on time through the solution of the circuit equations presented later*

The Joule heating $\dot{Q}_J$ is related to the current carrying capability of the conductor specified by the critical surface $J_c(B, T)$, of which two typical examples are reported in *Figure 1*. To remain as general as possible, we use the following method to compute the Joule heating term:

—for temperatures smaller than the current sharing temperature T_{cs}, no resistive loss will appear and

$$\dot{Q}_J = 0 \tag{9}$$

* The Joule heat generation in the composite conductor, in reality, will also depend on the current sharing transient. During the very early stage of the *current sharing* the current flowing in the superconductor exceeding the value of J_c will have to be transferred by inductive coupling and diffusion into the copper. This phenomenon, completely described by the Maxwell equations, is of extreme complexity. However, the characteristic time constant τ_c for the conductors considered here is of the order of hundreds of μs to some ms, while the quench characteristic times are between some tens of ms (initiation) to some tens of s (development). Therefore the current transfer can be assumed as a small perturbation and neglected. This is equivalent to the assumption of an instantaneous transfer ($\tau_c = 0$).

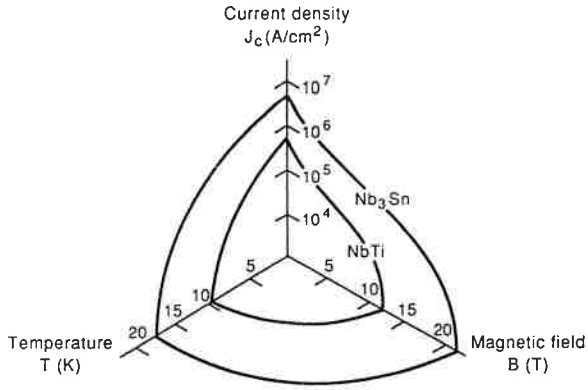

Figure 1 $J_c(B, T)$ surfaces for Nb_3Sn and NbTi

—for temperatures greater than the critical temperature T_c the whole loss will be concentrated in the copper

$$\dot{Q}_J = J^2 \rho_{Cu} \tag{10}$$

where ρ_{Cu} is the copper resistivity

—in the current sharing regime part of the loss will be in the copper and part in the superconductor. In this regime we can write that the total loss is

$$\dot{Q}_J = \frac{A_{Cu}\dot{Q}_{J_{cu}} + A_{sc}\dot{Q}_{J_{sc}}}{A_{Cu} + A_{sc}} \tag{11}$$

where the Joule heating in the copper is given by

$$\dot{Q}_{J_{cu}} = J_{Cu}^2 \rho_{Cu} \tag{12}$$

and the Joule heating in the superconductor

$$\dot{Q}_{J_{sc}} = J_{Cu}\rho_{Cu}J_c \tag{13}$$

where we used J_{Cu} to indicate the current density shared by the superconductor in the copper, i.e. if I is the operating current:

$$J_{Cu} = \frac{I - J_c A_{sc}}{A_{Cu}} \tag{14}$$

The term $J_{Cu}\rho_{Cu}$ is the electric field appearing along the cable due to the resistive current sharing in the stabilizer.

Note that using the assumption of linear dependence of J_c on T one obtains for $\dot{Q}_J$ the usual expression

$$\dot{Q}_J = g\left(\frac{I_{op}}{A_{Cu}}\right)^2 \rho_{Cu} \tag{15}$$

where

$$g = \begin{cases} 0 & \text{if } T < T_{cs}; \\ \dfrac{T - T_{cs}}{T_c - T_{cs}} & \text{if } T_{cs} \le T \le T_c; \\ 1 & \text{if } T > T_c \end{cases} \tag{16}$$

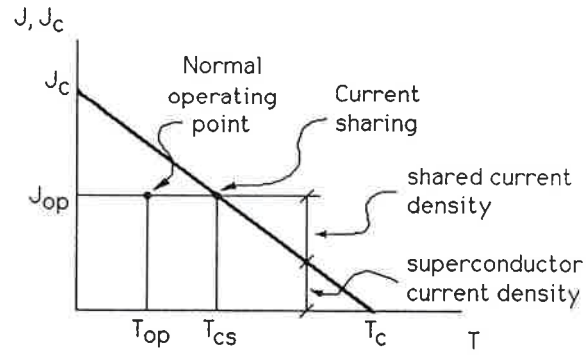

Figure 2 Operating point and definition of the current sharing temperature in the case of linear J_c *versus* T dependence. The effect of the increase of the operating temperature is also indicated by the shared current density

where the definition of T_{cs} is given in *Figure 2*. However, Equations (11)–(13) are valid for any dependence of J_c on T and B, while Equations (15) and (16) hold only in the case of linear J_c *versus* T dependence and should be, in principle, avoided if the J_c function is completely given. Finally, the copper resistivity ρ_{Cu} must le treated consistently in the calculation as a function of magnetic field and temperature.

Circuit equations. As shown above, the heat production term depends on the current flowing in the conductor, and this must be determined at any time by the solution of the electrical network formed by the pancakes in the inductively coupled coils and the external electrical components. In the case of a set of n inductively coupled coils, with independent power supply and dump resistors, the current I_i in the ith coil will be a function of time and of the currents in the other coupled circuits I_j through the differential equation

$$\sum_j M_{ij}\frac{dI_j}{dt} + L_i\frac{dI_i}{dt} + R_i I_i = V_i \tag{17}$$

where M_{ij} and L_i are the mutual and self inductances and R_i is the total resistance of the circuit. The first two are determined by the geometry of the circuit and will remain constant throughout the evolution of the quench. The term V_i is the voltage of the external power supply. Its value depends on the preprogrammed behaviour of the power supply and on the (V, I) characteristics.

The total resistance of each circuit is a function of time as it contains the contribution of the coil internal resistance R_{quench} which develops in time as the quench front propagates and the temperature changes. Further, due to the effect of magnetic field on copper resistivity, a change in the operating current in the magnet system will also affect the coil resistance.

Magnetic field in the coil

The magnetic field in the coil, B, can be computed using the Biot–Savart law. Usually the problem is linear function of the operating current of the magnets (no ferromagnetic materials), and the field can be computed using influence

matrices calculated at the beginning of the transient and stored. This increase greatly the efficiency of the calculation.

All the above equations need a consistent set of boundary and initial conditions. In particular, for the helium flow we assumed that the 1-D channels are connected to pressure reservoirs at inlet and outlet. The reservoirs represent manifolds with a large volume, but they can be assigned a pressure and temperature variation in time to model finite volume conditions. An alternative is a *symmetry* boundary condition on the flow, which also corresponds to a closed valve at the channel inlet or outlet. For the heat conduction equation, adiabatic boundaries are assumed around the coil, which is usually a sensible approximation of a well-shielded design. The calculation of the current requires the specification of the initial value of the current in the branches of the electric network, while for the magnetic field no boundary conditions are required (they are already satisfied by the Biot–Savart law).

Model

Without loss of generality, we consider the conductor configuration of *Figure 3*, representing a typical cable-in-conduit conductor[8], and the winding scheme in *Figure 4*. We can observe that the winding pack of a force-flow cooled superconducting coil presents a large anisotropy, in which we can clearly identify two main directions: the longitudinal axis of the conductor, characterized by a typical length of the order of hundreds of metres, and the transverse direction, normal to the longitudinal axis, which lies in the plane of the winding pack cross-section and with a typical length of the order of some centimetres. The modes of energy transport and propagation of a normal zone are substantially different in these two directions: in the longitudinal direction the helium flow is usually far more effective than heat conduction in propagating in the normal zone, while in the transverse direction heat conduction through cable jacket and insulation is the only mechanism responsible for the propagation. Finally, the thermal properties in the two directions are also largely

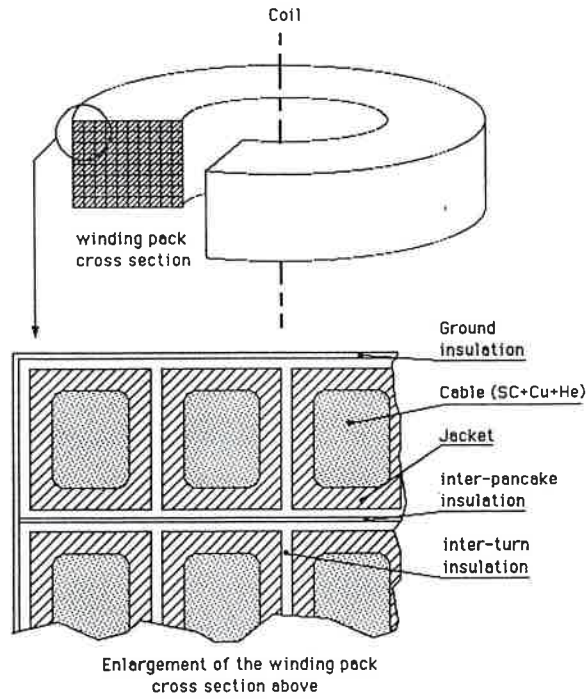

Figure 4 Schematic view of the winding pack configuration assumed

non-isotropic as the longitudinal heat conductivity of a cable is greater by several orders of magnitude than the transverse one.

It is natural to use these properties in the formulation of the computational model. In fact, the mere application of a brute force method, involving full meshing the 3-D domain, would be highly inefficient in terms of computational costs and could give serious numerical difficulties. The approach proposed here is to discretize the coil using a set of 1-D channels, and to couple these using an appropriate model of the transverse thermal resistance of the winding pack. A schematic view of this model is given in *Figure 5*.

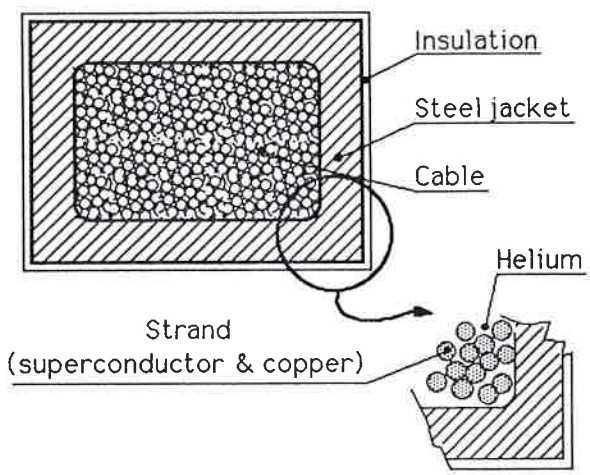

Figure 3 Schematic view of the cross-section of the conductor configuration assumed

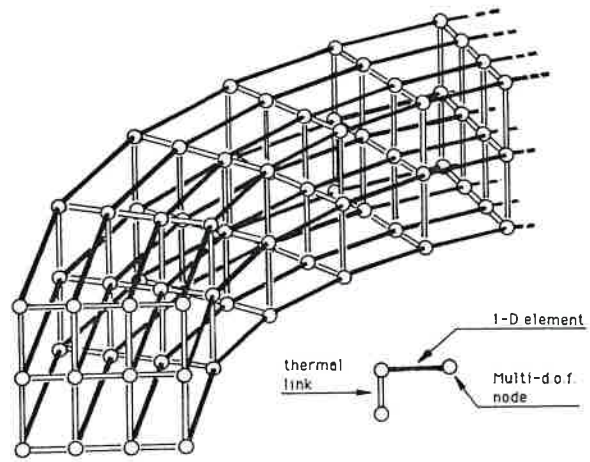

Figure 5 Approximation of the original 3-D problem with a set of coupled 1-D channels thermally linked in the cross-sections of the winding pack

Model for the 1-D channel

This is the basis of the quench analysis model, and consists of a 1-D representation of the cable in its longitudinal direction. Here the components forming the 1-D channel cross-section in which the helium flows are the superconducting strands and the assembly of jacket and insulation. The copper in the superconducting strand has a conductivity several orders of magnitude greater than that of the other components in the whole temperature range (from cryogenic temperature to room temperature). On the other hand the dominating heat capacities are those of the helium in the low temperature range (4 to 30 K) and those of steel and insulating materials (epoxy resins) in the high temperature range (30 K to room temperature).

Because of these differences in the material properties, it is not possible to combine all heat capacities and thermal conductivities. For instance, as the heat capacities change with temperature by several orders of magnitude in the range from 4 K to 50 K, the neglect of a small temperature gradient between the components of the strands in the cable (copper and superconductor) and the cable wall (jacket and insulation) could result in a large over-estimate of the total heat capacity of the cable. This is particularly true for cable-in-conduit conductors, where the steel and the surrounding insulation are not in direct, intimate thermal contact with the strands, but exchange heat mostly through the helium. In our model we assumed that the copper and superconductor in the strand have the same temperature by virtue of the large thermal conductivity of copper. At the same time the helium temperature in the channel will also be uniform, as in general the flow is highly turbulent and therefore involves a large degree of mixing. With regard to the jacket and insulation we approximated the temperature distribution by a uniform average temperature. The effects of the temperature gradients in the cable cross-section are taken into account, at least up to the first order, by separating the three components: strands, helium and jacket. The strands and the jacket are both in thermal contact with the helium, which acts as the main thermal coupling between them. In addition it is assumed that strands and jacket are in direct contact on a portion of their surface, thus adding a further thermal coupling term. The resulting model is simple to treat, and physically more realistic than that obtained by combining the heat capacities in one single point.

The model for the 1-D analysis is shown in *Figure 6*. The heat conduction equation (7) has to be converted into the following two equations for the strands and jacket respectively:

$$A_{st}\rho C_{st}\frac{\partial T_{st}}{\partial t} - A_{st}\frac{\partial}{\partial x}\left(K_{st}\frac{\partial T_{st}}{\partial x}\right) = h_1 S_{st-he}(T_{he} - T_{st}) + h_2 S_{st-jk}(T_{jk} - T_{st}) + A_{st}(\dot{Q}_{ext} + \dot{Q}_J) \quad (18)$$

$$A_{jk}\rho C_{jk}\frac{\partial T_{jk}}{\partial t} - A_{jk}\frac{\partial}{\partial x}\left(K_{jk}\frac{\partial T_{jk}}{\partial x}\right) = h_1 S_{jk-he}(T_{he} - T_{jk}) + h_2 S_{st-jk}(T_{st} - T_{jk}) \quad (19)$$

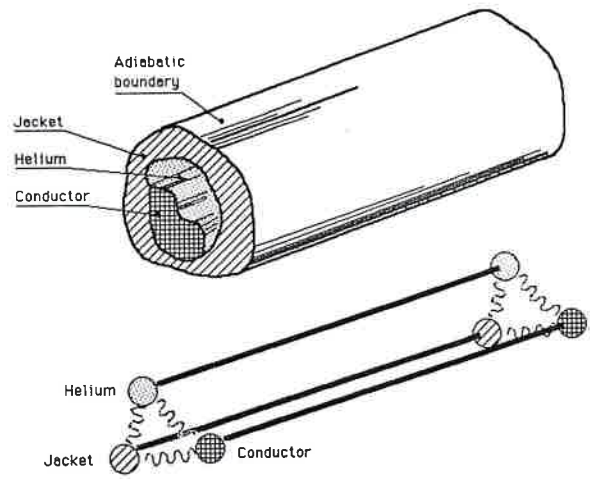

Figure 6 Schematic view of the 1-D model used for the conductor in the longitudinal direction

Equation (18) refers to the strand (subscript st), while Equation (19) is for the jacket and insulation (subscript jk). Note that for the contact to the helium and for the inner contacts of strands and jacket two different heat transfer coefficients have been used in the two equations above. In fact the heat transfer to the helium is substantially different from that at the contact surface between strands and jacket. The first, h_1, is defined using turbulent correlations, while the second, h_2, can be obtained only from measurements of thermal resistance and depends on the type of contact. Note also that in Equation (19) no source term has been included. In fact the external heating sources are usually located in the strands and the Joule heating in the jacket is negligible due to its high electrical resistivity at cryogenic temperatures.

The thermal properties for Equations (18) and (19) are obtained as weighted averages; in particular the density is given by the area weighted average of the densities of the single components

$$\rho = \frac{\Sigma_{i=1}^{n}\rho_i A_i}{\Sigma_{i=1}^{n} A_i}$$

The thermal conductivity is treated similarly

$$K = \frac{\Sigma_{i=1}^{n} K_i A_i}{\Sigma_{i=1}^{n} A_i}$$

while the heat capacity is given by the mass averages

$$C = \frac{\Sigma_{i=1}^{n}\rho_i C_i A_i}{\Sigma_{i=1}^{n}\rho_i A_i}$$

3-D model of the coil

The geometry of the jacket and the insulation between two adjacent cable spaces resembles very closely the situation of a composite slab. Therefore an approximation to the heat transfer in the winding pack can be

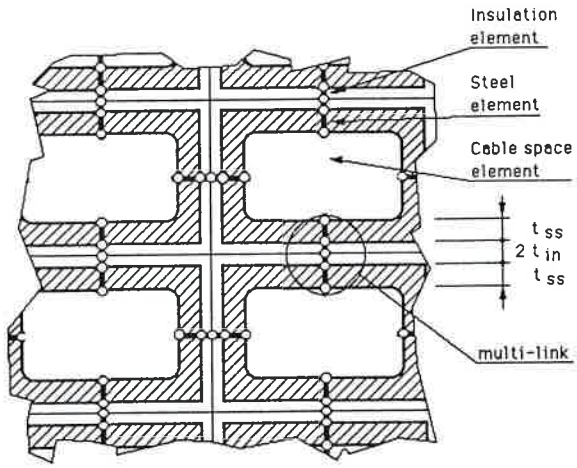

Figure 7 Equivalent multi-link model for the heat flux in the winding pack. The sandwich of jacket and insulation is substituted by a series of thermal resistances with degrees of freedom lumped at the centre of each layer of the sandwich

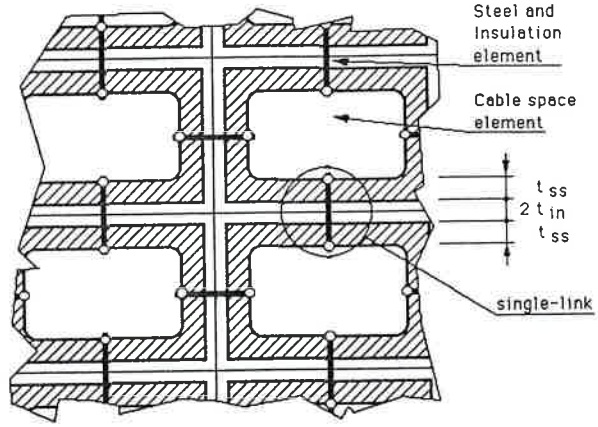

Figure 8 Equivalent single link model for the heat flux in the winding pack. This is the lowest level of approximation that can describe the heat flow between cables

obtained substituting each portion of jacket and insulation between two conductors with an equivalent slab having the same average length in the direction normal to the heat flux. With this simplification the heat diffusion in the winding cross-section can be regarded as a set of independent 1-D problems between the cable spaces.

The 3-D quench propagation can therefore be reduced to a set of 1-D problems with nodal links obtained through the heat conduction in 1-D through the composite slabs, as shown in *Figure 7*. The thermal links are located between nodes of adjacent turns in each pancake, and between nodes belonging to the same turn but in adjacent pancakes. Only conductors with adjacent faces are coupled, meaning that the heat flux across the corners of the cables is neglected.

The heat transfer in each composite slab presents a relatively easy problem, which could be solved again by discretization of the domain into finite elements. Nevertheless, it is advantageous to go further with the simplification, reducing the number of elements needed for the solution. Each multiple layer slab could be assimilated to a single layer link, with an equivalent heat conductivity, or thermal resistance, and heat capacity. The thermal resistance and the heat capacity should be chosen in such a way to guarantee the dynamic equivalence between multiple and single links, that is to say that both the steady state and transient effects on the temperature distribution should be considered in the lumping. The last level of approximation is therefore constituted by a set of 1-D channels cross-coupled, turn to turn and pancake to pancake, through a single layer link with given (non-linear) thermal resistance and heat capacity as shown in *Figure 8*. The amount of saving is clear, but two questions still have to be answered:

- How good is the approximation of 1-D heat flux in the jacket and insulation of each cable?
- How shall we choose the values of thermal properties of each link in order to get the response which resembles in a close manner that of the original system?

The answer to these two questions has to be sought in the fields of the substructuring[9] or model reduction techniques[10], as the procedure proposed consists of the reduction of the number of degrees of freedom of the problem.

Instead of using the rigorous formulation of the problem let us come back again to the simple analogy with the 1-D slab. In steady state conditions, assuming that the properties are linear it is possible to define the heat resistance of the 1-D slab as

$$h = \frac{1}{\Sigma_i \frac{L_i}{K_i}} \tag{20}$$

and the heat flux through the slab is equal to

$$\dot{q}'' = h\Delta T \tag{21}$$

where ΔT is the temperature difference across the slab. For a steady state non-linear problem it is possible to use a reasonable approximation of the thermal resistance by performing a further subdivision of the slab in portions with nearly constant thermal conductivity. The limit of this procedure is the differential equivalent of Equation (20).

$$h = \frac{1}{\int_x \frac{dx}{K(x)}} \tag{22}$$

Although these simple results are only valid in steady state conditions, we can assume that they give a good approximation of the dynamic behaviour in the time scale of interest. In fact, during a transient, the temperature distribution and the heat flux will tend asymptotically to the steady state solution. In this aspect, the steady state can be regarded as the mode with the lowest frequency (apart from the thermal equivalent of

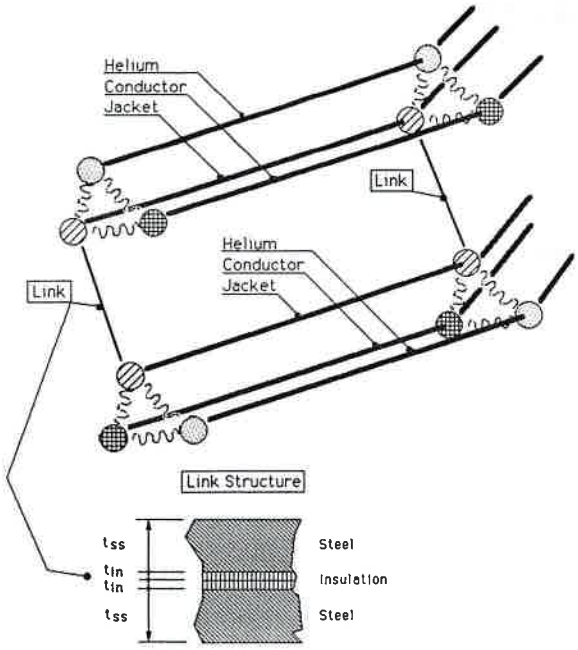

Figure 9 Schematic view of the details of the coupled 1-D channels equivalent to the initial 3-D problem. The internal structure of the coupling links is shown

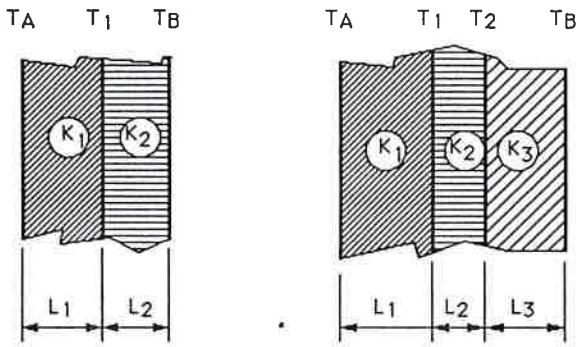

Figure 10 Configurations considered for the calculations of the thermal resistance of the links. The values of the temperature at the boundaries of the slab are given

a rigid body displacement). Tests performed in relevant geometries and under relevant initial boundary conditions have shown that the situation can be closely modelled by a 1-D slab in steady state[11,12].

A detailed view of the resulting model for the coil is given in *Figure 9*, where the structure already shown in *Figure 5* is expanded.

For the calculation of the value of the thermal resistance of the link, two types of composite structure have been considered: a two-layer slab and a three-layer slab. The first is the case of two cables in direct contact at their jackets, the second that of the jacket–insulation–jacket sandwich. Given the temperature at the boundaries of the slab, T_A and T_B in *Figure 10*, the steady state value of the temperature in the interior points is easily calculated in the approximation of linear properties. In the case of the two-layer composite, we have

$$T_1 = \frac{\dfrac{K_1}{L_1} T_A + \dfrac{K_2}{L_2} T_B}{\dfrac{K_1}{L_1} + \dfrac{K_2}{L_2}} \tag{23}$$

while for the three-layer composite

$$T_1 = \frac{\dfrac{K_1 K_2}{L_1 L_2} T_A + \dfrac{K_1 K_3}{L_1 L_3} T_A + \dfrac{K_2 K_3}{L_2 L_3} T_B}{\dfrac{K_1 K_2}{L_1 L_2} + \dfrac{K_1 K_3}{L_1 L_3} + \dfrac{K_2 K_3}{L_2 L_3}} \tag{24}$$

$$T_2 = \frac{\dfrac{K_1 K_2}{L_1 L_2} T_A + \dfrac{K_1 K_3}{L_1 L_3} T_B + \dfrac{K_2 K_3}{L_2 L_3} T_B}{\dfrac{K_1 K_2}{L_1 L_2} + \dfrac{K_1 K_3}{L_1 L_3} + \dfrac{K_2 K_3}{L_2 L_3}} \tag{25}$$

Once the temperature at the interior is known, it is possible to compute the value of the average thermal conductivity of each layer. To simplify matters, the value of K is computed at the average temperature of the layer. In fact the solution of Equation (23) or of Equations (24) and (25) requires an iterative procedure. Direct iteration can be performed quite efficiently (generally three to four iterations are enough to reach a relative error of less than 10^{-3} of the heat flux). Once the solution has converged the thermal resistance is computed using Equation (20). This is finally used to compute the equivalent heat transfer between adjacent conductor jackets, according to Equation (21).

Initial conditions

The initial condition for a coil in which a quench starts is, in general, that of normal operation. The coil is cooled by a steady flow of helium under given heat loads. In the model considered here the distribution of the variables should be computed along the channel. As we have chosen an explicit solution method for the helium flow a relaxation procedure could be used letting an initial, arbitrary distribution (e.g. zero flow) evolve to the natural steady state. This is feasible but time consuming, as the time stepping should cover at least a couple of residence times of the coolant in the cooling path to achieve a steady state condition. Therefore an approximation is used for the determination of the initial steady state distribution in the channel. Neglecting all the time derivatives in Equations (1)–(3) and assuming that the heat diffusion in the conductor (Equations (18) and (19)) is negligible, the resulting set of equations is much easier to solve: the mass flow is constant (from the steady state continuity equation), and for relatively small flows (as in typical technical applications) the pressure drop is given by

$$\frac{\partial p}{\partial x} \approx 2f \frac{\rho v^2}{D_h} \tag{26}$$

where the compressibility effects have been neglected. The energy equation can be written in terms of enthalpy of the fluid $h = i - (p/\rho)$

$$\dot{m}\frac{\partial h}{\partial x} \approx A_c \dot{Q}_{ext} \tag{27}$$

where again the compressibility terms have been neglected. An approximate solution of the two equations above can be achieved assuming that the r.h.s. of Equation (26) is constant along the pipe length. In this case the pressure distribution is linear along the length and the pressure drop is given by

$$\Delta p = 2f\frac{\rho v^2}{D_h} L \tag{28}$$

where L is the pipe length. The enthalpy distribution is also easily computed from Equation (27) by integration of the external heating, which is an assigned function of space. The local values of pressure and enthalpy uniquely determine all the other variables of the helium. Helium temperature and density are therefore known, and the latter can be used to determine the flow velocity in the assumption of constant mass flow. The conductor temperature is then set equal to that of helium, assuming that in steady state the temperature gradients between conductor and helium must be small.

Method of solution

For the solution of the helium flow and of the heat conduction along the conductor longitudinal axis we used the finite element method[13] (FEM). This has the advantage of giving higher accuracy and more modelling freedom than, for instance, the finite difference approximations of the governing equations. The 1-D model of the cable cross-section was translated into a finite element with three thermal degrees of freedom per node: strand, helium and jacket temperature. In addition to these, the flow variables were defined at the helium nodes. The 1-D channels were obtained by assembly of these elements. Note that the element can be easily modified to take into account other conductor configurations, e.g. the case of several independent cooling channels in the conductor, or to model better the jacket structure, subdividing it into layers of steel and insulation[6].

The solution of the helium flow was based on an explicit two-step form of the Taylor–Galerkin algorithm[12–14], which offered optimal compromises among accuracy of the integration, CPU cost and programming simplicity. For the heat conduction equation an implicit solver was used. Implicit treatment was implemented also in the heat exchange among the components of the 1-D element, while explicit coupling was used among the channels, to form the 3-D assembly. This choice was justified by the fact that the time constants of the heat transfer with the helium are very small (of the order of one millisecond) compared to those of the heat transfer among conductors in the winding pack (typically some tenths of a second). Therefore, the simplification of the data structure was obtained without major penalties due to the conditional stability of the explicit parts of the solution algorithm. In fact, the strictest requirements on the time step were dictated by the algorithm used in the solution of the helium flow.

The circuit equations were solved by standard techniques adopted in initial values and ordinary differential equations, and the coupling to the thermal-hydraulic analysis was achieved explicitly. This also posed no serious problem for stability and consistency of the algorithm, as the time constants of the electrical circuits modelled are in general several orders of magnitude larger than those involved in the quench propagation. Finally, the magnetic field was computed at each time step by means of preprocessed influence matrices, whose coefficients link the field at any point to the current in the circuital branch.

The final algorithm could be broken in modules performed independently at each time step, so that there is a great potential for parallel processing and speed increase. In fact, great attention was devoted to achieving a sufficient CPU speed to allow dealing with very large problems arising when a whole coil is modelled. Material properties and helium property routines were also subject to this optimization process to guarantee that even with extremely large problems (e.g. a complete coil) a solution could be obtained in reasonable computing time (some CPU hours).

Conclusion

The model presented for the analysis of quench in superconducting, force-flow cooled magnets advances substantially those previously used as it allows inspection of the thermal gradients in the cable and includes transverse heat transfer among conductors in the winding pack. The solution of the coupled heat diffusion and helium flow has been successfully reduced to sets of simplified coupled 1-D problems equivalent to the original configuration. The formulation of the 1-D problem given here is appropriate for the analysis of a coil wound from cable-in-conduit conductors. A treatment similar to that proposed here could be used to extend the 1-D model to other situations, e.g. other conductor configurations, provided that the 1-D analogue is a good description of the original 3-D problem.

The method proposed has been implemented into a code which is able to solve the full problem of the quench propagation in a 3-D configuration, also taking into account the operating current and magnetic field changes by means of integrated circuital and magnetostatic solvers. We believe that at the moment this is the most versatile and comprehensive simulation model for force-flow cooled superconducting magnets. An extensive numerical and experimental validation program is under way to check that the assumptions and the solution algorithms have a sound physical basis. Part II of this paper gives examples of applications in relevant conditions.

References

1 **Wilson, M.N.** *Superconducting Magnets*. Clarendon Press, Oxford (1983)
2 The Next European Torus (NET) *Fusion Technol* (1988) **14** 1
3 **Arp, V.** Computer analysis of quench transients in force-flow cooled superconductors for large MHD magnets *Proc Superconducting MHD Magnet Design Conference*, MIT, Cambridge (1978)

4 **Marinucci, C.** A numerical model for the analysis of stability and quench characteristics of force-cooled superconductors *Cryogenics* (1983) **23** 579–586

5 **Cornelissen, M.C.M. and Hoogendoorn, C.J.** Propagation velocity for a force cooled superconductor *Cryogenics* (1985) **25** 185–193

6 **Wong, R.L.** Program CICC flow and heat transfer in cable-in-conduit conductors, presented at 13th Symp. on Fus. Eng., Knoxville, TN (October 2–6, 1989)

7 **Luongo, C.A., Loyid, R.J., Chen F.K. and Peck, S.D.** Thermal-hydraulic simulation of helium expulsion from a cable-in-conduit conductor, *IEEE Trans Magn* (1989) **25** 1589–1595

8 **Hoenig, M., Iwasa, Y. and Montgomery, D.B.** Supercritical-helium cooled 'bundle conductors' and their applications to large superconducting magnets *Proc 5th Int Conf on Magnet Technology*, Frascati (1975)

9 **Guyan, R.J.** Reduction of stiffness and mass matrices *AIAA J* (1965) **3** 380

10 **Ben Jaafar, M.T., Pasquetti, R. and Petit, D.** Model reduction for thermal diffusion: application of the Eitelberg, Marshall and aggregation methods to a heat transfer transmission tube model. *Int J Numer Meth Eng* (1990) **29** 599–617

11 **Bottura, L.** 2-D simulation of quench propagation for force-flow conductors *IEEE Trans Magn* (1991) **27** 1904–1907

12 **Bottura, L.** The numerical solution of quench in superconducting magnets. *PhD Thesis* submitted to the University of Wales, University College of Swansea, Wales, UK (1991)

13 **Zienkiewicz, O.C. and Taylor, R.L.** *The Finite Element Method*, Vols 1 and 2, 4th Edn McGraw Hill, New York (1989–1991)

14 **Peraire, J., Peiro, J., Formaggia, L., Morgan, K. and Zienkiewicz, O.C.** Finite element Euler computations in three dimensions, *Int J Numer Meth Eng* (1988) **26** 2135–2159

Quench analysis of large superconducting magnets. Part II: model validation and application

L. Bottura and O.C. Zienkiewicz*

The NET Team, c/o Max Planck IPP, Boltzmannst. 2, D-8046 Garching, Germany
*Institute for Numerical Methods in Engineering, University College of Swansea, Swansea SA2 8PP, UK

Received 26 September 1991; revised 13 January 1992

We report here the results of some applications of the 3-D quench propagation model presented in Part I of this paper. Various validation runs based on experimental data are presented. Most of these are in 1-D geometry, and were used to check the accuracy of the computer code in simplified conditions. However, we also show here the 3-D simulation of the quench jump observed in the tests of the EU-LCT coil at Oak Ridge, which we used as an integral test of the 3-D capability of the code. Finally we report the results of an application of the computer code to the verification of the protection of the NET model coil. For this last case, the full capability of the 3-D model is used in simulation of the quench propagation in two conditions: when the coil is dumped on the fast discharge circuit and in the event of a short circuit of a coil module.

Keywords: quench, protection, force-flow superconductors

In Part I of this paper[1] we presented a model for the simulation of the quench of a superconducting, force-flow cooled magnet. The model is based on the assumption that the winding pack of the coil can be treated as an assembly of 1-D channels coupled through thermal resistances. The 1-D channels describe the details of the conductor cross-section, while the thermal resistances are chosen to be equivalent, in a dynamic sense, to the heat fluxes in the winding pack cross-section.

The complexity of the problem, and the associated non-linearity, pose a serious problem to the validation of any numerical method used for its solution. This is specially the case for the solution of the flow equations. Here, apart from very simple test runs, performed for perfect gas or linearized state equations, very few checks are possible in real conditions. This is even more true when the coupled problem is considered. Therefore only an experimental comparison can prove, at least partially, the reliability of the code. In this paper the results of some experiments performed on helium cooled pipes and conductors are used as benchmarks to test the accuracy of the method. These experiments have been chosen for the good definition of the conditions and history of the most interesting variables, in particular pressure and temperature of the helium. Good documentation is available from all the experiments in the references indicated, and here only a brief sketch of the set-up is given in order to understand better the simulation. An integral test of the 3-D model was performed using the data generated during the quench jump observed in the testing of the EU-LCT coil. Finally, we show an application of the 3-D model to the NET model coil design during a coil dump from normal operating condition and with a coil module shorted.

0011 – 2275/92/080719 – 10

Validation runs

The HELITEX experiment

The first experiment chosen is the one performed in 1980 by Benkowitsch and Krafft[2,3]. They did series of experimental runs in order to assess the magnitude of the heating induced flow of helium in long channels. These experiments were performed in the HELITEX facility at KfK, Karlsruhe.

Experimental set-up and data. The experiment consisted of the transient heating of a spirally wound channel of 30 m length and 4 mm^2 cross-section, filled with liquid helium at 4.1 K at 1 bar* (see *Figure 1*). Once the initial conditions of pressure and temperature were

*1 bar = 10^5 Pa

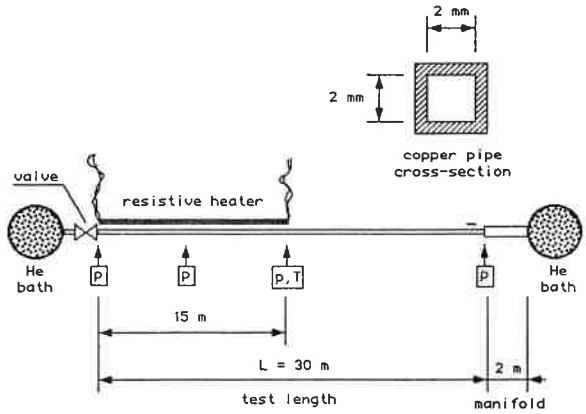

Figure 1 Schematic view of the apparatus and conditions for the HELITEX experiment[2,3] with heater location and cross-section of the copper pipe. The location and type of sensors are also shown (small boxes)

established, the valve at the inlet was closed and the shot started.

The heating was obtained by discharging a bank of capacitors into a 15 m long resistive strip which was thermally coupled to the channel. The total deposited energy was inferred from the initial charge of the capacitors. Since the thickness of the tube wall was small, and its heat capacity negligible compared to that of the helium contained, the heat transfer into the solid and from the solid to the helium was neglected. In reality the presence of the pipe walls modified the time constant of the heat deposition in the helium. This effect was estimated by Benkowitsch[2] assuming the following dependence of the power on time:

$$\dot{Q}(t) = \begin{cases} \dot{Q}_0 \dfrac{t}{t_1} & \text{for } t \le t_1 \\ \dot{Q}_0 \, e^{(t_1 - t)/\tau} & \text{for } t > t_1 \end{cases}$$

The values of Q_0, t_1 and τ depended on the total energy deposited in the channel. Several runs were performed at different levels of deposited energy and using different time constants for the capacitor's discharge. However, due to the rather large time constant for the energy transfer to the helium, the values of t_1 and τ showed experimentally only a slight dependence on the energy. Therefore they have been chosen here as fixed for any value of the total energy, as estimated by Benkowitsch[2].

The friction factor was measured by steady state pressure drop experiments, and, neglecting the influence of the pipe curvature, it is described by the following relation, in the laminar regime

$$f = \frac{7}{8}\frac{16.0}{Re}$$

and, in the turbulent regime, by

$$f = \frac{7}{8}\frac{0.076}{Re^{0.25}}$$

The transition between the laminar and turbulent regimes is at about $Re = 1250$. The multiplicative coefficient 7/8 takes into account the shape effects due to the square cross-section of the channel[2,3].

Pressure and temperature sensors were placed every 7.5 m in the test section. Good quality traces were generated for the pressure, while the temperature sensors generally registered the variation in the helium with a delay and an attenuation probably due to the insufficient thermal coupling. Unluckily no other sensors, such as mass flow meters, were included. It appears therefore that the only reliable measurements were those of the pressure.

Experimental results and simulations. The heating of the helium generated a pressure and temperature increase in the heated region and a pressure wave travelling downstream. This wave travelled at sonic speed up to the end of the test section, and it could be sensed as a delay in the pressure increase for the sensors out of the heated region. The maximum pressures, reached at times between 300 and 350 ms after the beginning of the 'shot', showed a clear correlation with the input energy. The same was true for the maximum temperatures in the heated region, although, as said before, these measurements were much less reliable.

For the simulation, the pipe was modelled with different meshes of increasing refinement, consisting of 32, 64 and 128 elements respectively. The modelled length was 32 m, as an additional piece of 2 m length was added to simulate the manifold at the outlet. Obviously the best results, reported here, were obtained with the finest mesh. However, the size of the elements had the main influence on the smoothness of the solution, with practically no effect on the values of maximum pressure and temperature at the centre of the pipe.

In *Figure 2* the pressure computed in the locations corresponding to the sensors is shown. The agreement with the experimental measurements is very good for both the sensors at $x = 0$ m and $x = 15$ m, while some mismatch appears for the sensor at $x = 30$ m. This is certainly due to the effect of the boundary conditions: as mentioned above, the test section was connected to a manifold, and this has been only crudely simulated by attaching an additional piece of pipe in the model. Note, however, that the delay in the arrival time of the pressure wave is correctly simulated. For comparison, the isochoric solution for the pressure increase is reported for the first sensor, at $x = 0$ m, showing that only during the early stage of the heating, for times smaller than about 50 ms, does the system follow an isochoric process. The reason is that at the beginning of the evolution there is no net outflow at the extreme of the heated region. The time at which the ideal isochoric behaviour and the real evolution start to diverge is again determined by the sonic speed in the helium, since the information on the boundary condition at the end of the heated region has to travel up to the pipe end to produce a net mass flow.

The temperature in the sensor at $x = 15$ m was also compared to the experimental measurements but, as in the case of the simulation performed by Benkowitsch[2], a clear disagreement was found. The measurement shows a delay in the response with no theoretical justification. A defect in the sensor installation, as

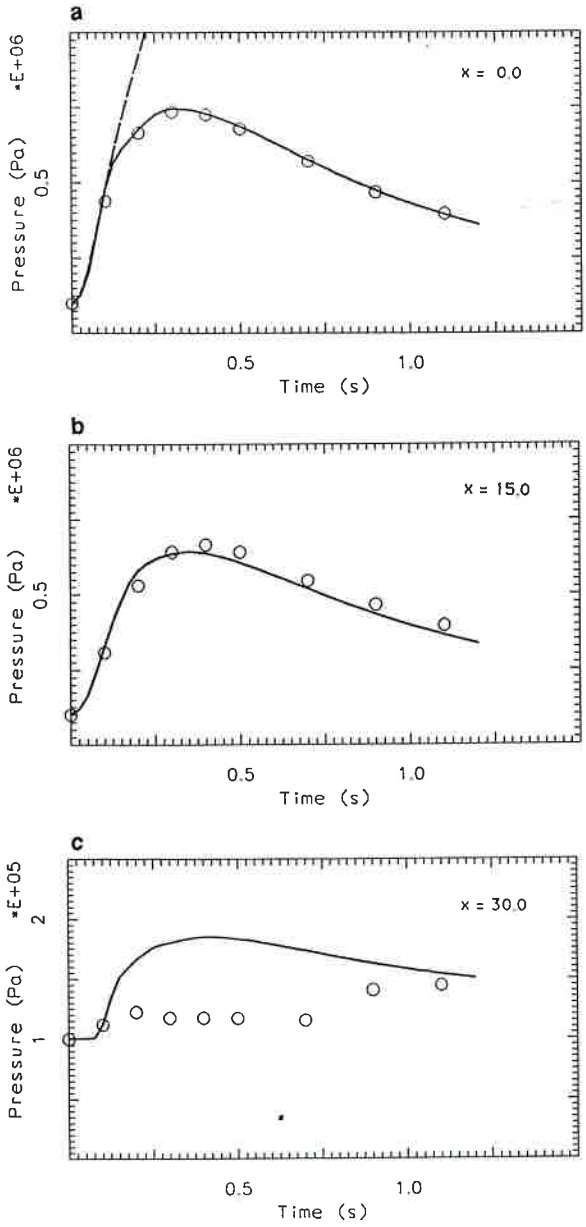

Figure 2 Comparison of computed (solid line) and experimentally measured (circles) pressure at the sensors. The isochoric pressure calculation is superimposed (dashed line) for the $x = 0$ sensor

suggested by Benkowitsch[2], is the most probable explanation.

Changing the total deposited energy in the simulation, it is possible to compare the computed maximum pressure at the sensors with the experimental measurements over the whole experimental range. This has been done in *Figure 3*, showing in general good agreement between calculation and experiment. A deviation is observed for the sensor at $x = 0$ at high energy, and this is probably due to the influence of the heat capacity of the valve and the neighbouring helium on the actual thermal mass at the sensor. A heat leak through the boundary would decrease the temperature and pressure at the

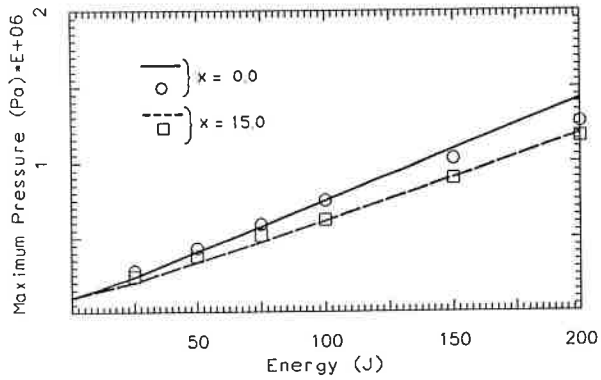

Figure 3 Maximum pressure as a function of the total deposited energy at two sensors. The lines represent calculation results, while the symbols (circles and squares) are the measured values

sensor. Furthermore, the value of the time constants of the energy deposition might depend on the absolute amount of energy deposited and this has an influence on the maximum pressure.

Pressure increase experiments by Lue et al.

A more complete verification of the code was possible using the data generated by Lue *et al.* in the period 1980–82[4,5]. This experiment is more significant as it simulates the quench of a long length of conductor including the Joule heat generation process in a normal conducting material.

Experimental set-up and data. The 69 m long conductor was constructed by cabling 0.693 mm diameter copper strands. The cable was inserted into a 304 SS tube, which was compacted afterwards to a final outer diameter of 5.2 mm and 0.4 mm wall thickness. The conductor was wound around a 100 mm thick PVC mandrel and placed into a stainless steel Dewar, filling the void between mandrel and Dewar with epoxy resin. As the heat capacity of the epoxy resin is rather high compared to that of the metallic materials at 4 K, it had to be included in the heat balance equation of the solid. In addition the intimate thermal contact between the test section and the supports might be the cause of some heat leak which could not be modelled in the following simulations.

The quench was simulated using a fast response current supply, providing a pre-programmed current rise in the circuit within 0.1 ms and holding it for a time τ_1. In some cases an exponential decay with a time constant τ_2 followed the plateau of the current, to simulate the dump of a coil. Since no superconductor was included in the strands, the Joule heating was uniform along the length. Strictly speaking, no propagation took place, as the whole conductor was normal from the beginning. One end of the conductor was always open into a constant pressure ambient, while the other end could be either open or closed (simulating in the last case a conductor length of 138 m with both ends open).

Considering the different combinations of operating currents and boundary conditions, a total of eight experimental runs have been examined for the conditions given in *Table 1*.

Table 1 Experimental conditions for the 8 runs used for the comparison with the simulations

Run number	End condition	Length simulated (m)	Current (A)	τ_1 (s)	τ_2 (s)
1	Open	69	760	3	0
2	Open	69	940	5	0
3	Open	69	1250	6.7	0
4	Open	69	940	3	9
5	Closed	138	760	6.7	0
6	Closed	138	940	6.7	0
7	Closed	138	1250	6.7	0
8	Closed	138	1540	6.7	0

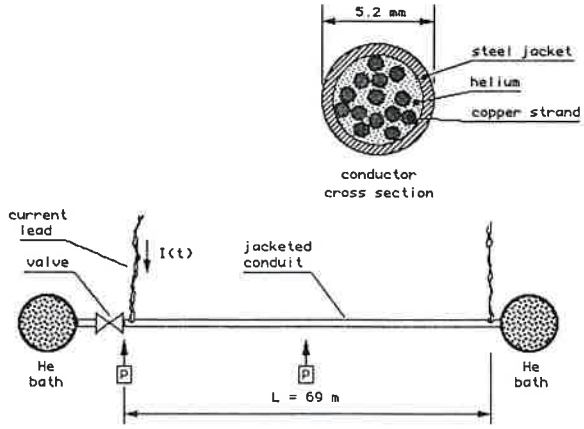

Figure 4 Schematic view of the set up of the Lue *et al.* experiment[4,5] with the cross-section of the jacketed copper conductor. The location of some pressure sensors is also shown (small boxes)

For the cable used in the experiment the friction factor was considerably different from that used for a smooth tube. This is due to the increased turbulence induced by the cable structure (triplets). Experimental measurements showed that for a triplexed cable the friction factor can be 3 to 6 times higher than for a smooth tube at the same Reynolds number[6]. Experimental data have been correlated by Hooper[7] into the following expressions:

$$f = \begin{cases} \dfrac{16}{Re} & \text{for } Re \le 99.73 \\ \exp\left(\dfrac{13.15}{Re^{0.36}} - 4.338\right) & \text{for } Re > 99.73 \end{cases}$$

The heat transfer coefficient between helium and conductor in the turbulent regime is computed as a combination of the steady state component, given by a modified Dittus–Bölter correlation

$$h_s = \frac{K}{D_h}\, 0.0259\, Re^{0.8} Pr^{0.4} \left(\frac{T_{he}}{T_s}\right)^{0.716}$$

and a boundary layer diffusion term

$$h_t = \sqrt{\frac{K\rho C_p}{\pi t}}$$

The two are combined as parallel heat transfer paths:

$$h = h_t + h_s$$

In the laminar regime the Nusselt number is limited to a minimum value corresponding to the laminar heat transfer coefficient in an annulus[8]

$$Nu_{min} = \frac{h_{min} D_h}{K} = 8.235$$

Finally, the residual resistivity ratio (*RRR*) of copper has been taken equal to 80, according to the resistivity measurements at low temperature. Some uncertainties are connected with the temperature dependence of the resistivity, resulting in imprecision in the description of the Joule heat generated.

Experimental results and simulations. The temperature and pressure in the conductor showed a rapid increase in the first instants of the pulse. For the pressure, this first phase was followed by a change in the slope, where the increase of the pressure slowed down until, eventually, a peak was reached and the pressure started decreasing. In the first phase the pressure and temperature rose following the Joule heat deposition as if the process were at constant volume. The change in the pressure increase rate was due to the effect of the strong induced flow, which could be established at any point only after the arrival of the pressure wave from the outlet. This helium expulsion from the heated cable relieves the pressure until at a certain point this last tends to decrease. The instant when the maximum is reached depends on the length of the channel. The temperature in the conductor, on the other hand, keeps increasing at almost constant rate while the heating is on. Little influence of the conductor length and flow characteristics is observed, meaning that a locally adiabatic hypothesis seems reasonable.

The pressure in the centre of the conduit has been computed as a function of time and compared to the experimental traces in *Figures 5* and *6*. In general the agreement is good in the first instants of the evolution. Some substantial deviation appears for longer times and at low operating current. The reason for the disagreement of experiments and calculations can be identified in three points:

1 The uncertainties in the material properties. Most important is the resistivity of copper, which influences the heat production term.
2 The complexity of the heat flow path. The model used here might be insufficient to describe the heat flow in the epoxy filler.
3 The assumption on the flow boundary. In the experimental runs a pressure increase at the outflow of the order of 0.5 to 1 MPa was observed, but in the simulation the pressure at the boundary was taken con-

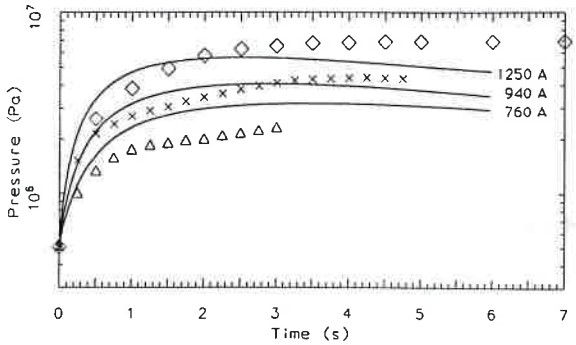

Figure 5 Comparison of experimental measurements (symbols) and simulations (solid lines) of the pressure increase in the centre of the conductor for a conductor length of 69 m (open valve at the conductor end) at different currents

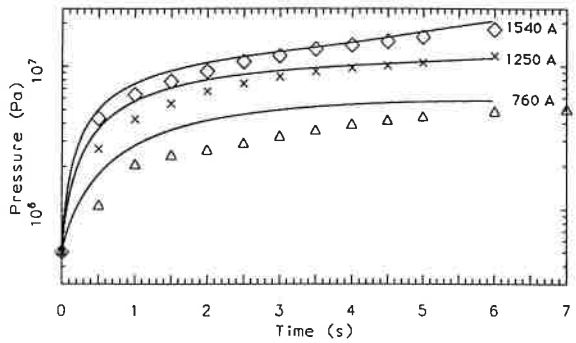

Figure 6 Comparison of experimental measurements (symbols) and simulations (solid lines) of the pressure increase in the centre of the conductor for a conductor length of 138 m (closed valve at the conductor end) at different currents

stant in time. The boundary effects should be more evident for short test lengths and long times. This can partially explain the deviation between the experiment and the simulation that is evident in *Figure 5* for times above 3 s, when the simulation shows a slight pressure decrease while the measured pressure remains nearly constant.

A better agreement is found on the temperature traces in *Figure 7*, where the experimental and computed

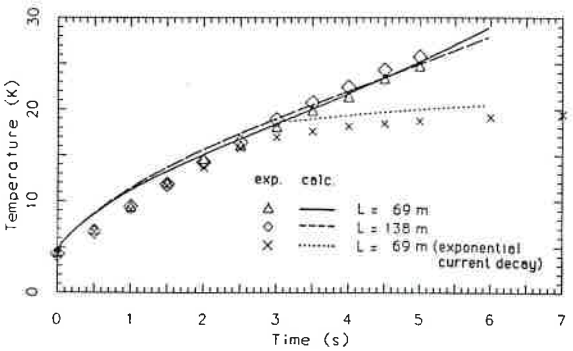

Figure 7 Comparison of experimentally measured and computed temperatures in the centre of the conductor for different pulses. The operating current is 940 A

values are compared. No significant difference can be noted between the two runs at 69 and 138 m length, as should be expected. The heating of the conductor is locally adiabatic, and the temperature evolution should depend only on the locally available heat capacity.

EU-LCT quench jump experiment

Among several tests performed on the LCT coils at ORNL[9] (Oak Ridge National Laboratory), one in particular was dedicated to the measurement of the time needed for a quench to jump from one turn to the next through heat conduction[10]. This is exactly the mechanism being investigated here, and therefore the experimental conditions have been used to benchmark the several approximations proposed. As described in Reference 9, the EU-LCT coil was wound in double pancakes using the two-in-hand technique. This allowed the use of the two conductor lengths of a double pancake as branches of a compensated resistive bridge for quench detection. The quench jump from the first conductor length to the second one could be determined both by the appearance of a resistive voltage across the second conductor length and by the decrease of the total compensated voltage. The experimental results are limited to the measurements of the resistive voltage in each pancake and of the total compensated voltage. Almost no data exist on the local temperature in the conductor. However, the time needed for the quench jump is very well defined in the experimental traces. This is the parameter used for the comparison of the results of the simulations.

Simulation model and results. The EU-LCT coil was initially operated at 8 kA current with an inlet temperature in the winding pack of 3.77 K at a pressure of 1.1 MPa. The helium at the inlet of one of the two conductor lengths of double pancake 7 was then heated for some seconds above the current sharing temperature of the conductor, i.e. to about 7.5 K. A quench initiated at the inlet of the conductor and propagated along its length. As a consequence an increasing resistance appeared across the first half of the double pancake. The measurements continued until a second quench was initiated by conduction in the neighbouring conductor length of pancake 7, after 8 s.

The simulation was performed on one double pancake only, assuming that the contribution of the adjacent double pancakes and of the coil casing was negligible. Inlet pressure, temperature and mass flow were used to establish the steady state conditions for the analysis.

In fact only the first two turns of double pancake 7 were modelled, using a total of 110 elements along the length. Constant pressure boundary conditions at the helium inlet and outlet (large reservoir) were imposed (see also *Figure 8*). At one of the two helium inlets of the double pancake a heated fluid slug was simulated, increasing the helium temperature in the boundary reservoir to 7.5 K for 5 s and then ramping it down to the initial value in 3 s.

The simulation starts from the initial steady state condition and ends at about 10 s after the initiation of the quench in the first conductor length. As shown in *Figure 9*, the temperature in the first conductor rises slowly following the hot helium injection to about 5 s from the simulation start. At this point the current shar-

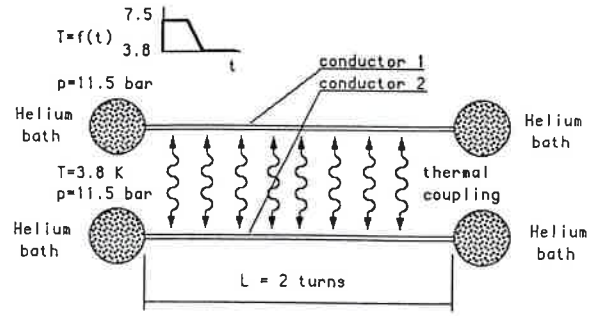

Figure 8 A schematic view of the simplified configuration used for the simulation of the EU-LCT quench-jump experiment

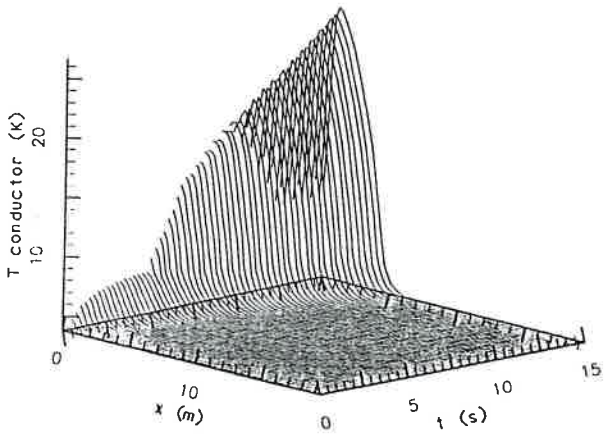

Figure 9 Temperature evolution in the first two turns of the first conductor (initially quenched) computed in the simulation of the EU-LCT quench-jump experiment

ing temperature is reached and the quench of the first conductor starts. This is marked by the strong temperature increase in *Figure 9*. As the first quench starts, the temperature in the second conductor length begins to increase considerably, as shown in *Figure 10*,

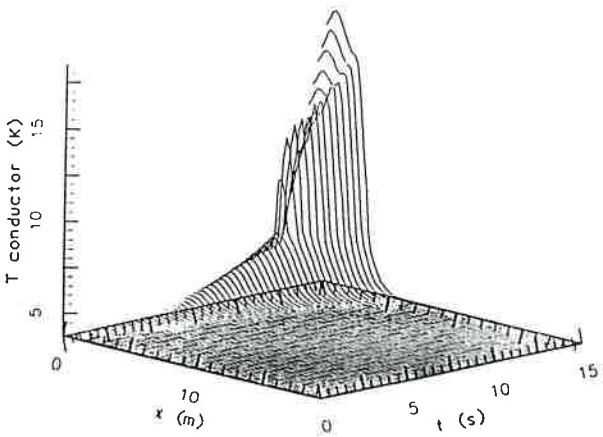

Figure 10 Temperature evolution in the first two turns of the second conductor (initially not perturbed) computed in the simulation of the EU-LCT quench-jump experiment

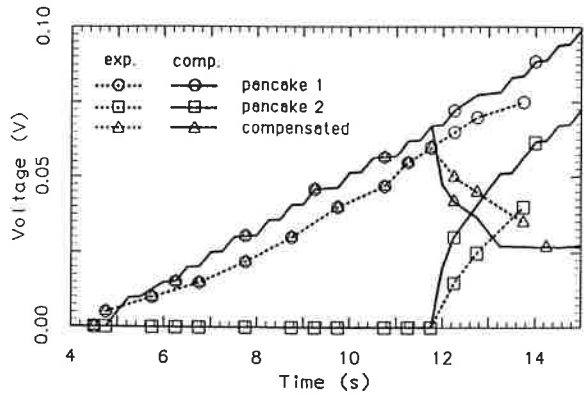

Figure 11 Computed and experimentally measured voltages in the EU-LCT quench-jump experiment. The experimental curves have been shifted in time so that the quench jump happens at the same instant

due to the thermal conduction through the jacket and insulation. At about 12 s the second conductor length in the double pancake also reaches locally the current sharing state and the induced quench starts. The computed delay between the initial and induced quench compares very well with the measured value, about 7 s and 8 s respectively.

The voltage traces computed by the code are compared to the values measured during the experiment as shown in *Figure 11*. The latter have been offset in time, so that the second quench starts at the same time. The computed voltage increase rate in both pancakes' halves is very close to the measured values, as well as the quench jump time. The differences on the voltage might possibly be due to uncertainties in the copper resistivity and RRR values. The compensated voltage (difference of the voltages in the two halves of the double pancake) reaches a peak and then decreases as observed experimentally. The decrease is due to the fact that the quench in the second half of the double pancake propagates initially quicker than in the first half because of the pre-heating of the helium. Also this effect is clearly predicted by the simulation.

The code predicts the quench jump quite accurately, despite the many uncertainties regarding the conductor parameters and the fact that the boundary conditions can play an important role. This is indeed very encouraging, as the conditions of this experiment are exactly representative of the field of future application for the code. However, it has to be recognized that the spectrum of comparison is limited by the fact that the measurements on the coil were scarce and the sensors could respond only in a slow time scale.

An application: quench of the NET model coil

The NET model coil[11], shown in *Figure 12*, will be an integral test of the concepts of the superconducting cables developed for the NET toroidal and poloidal field coils (TF and PF coils respectively). Therefore the experimental runs will have as a principal objective the exploration of the ultimate operating limits of the coil

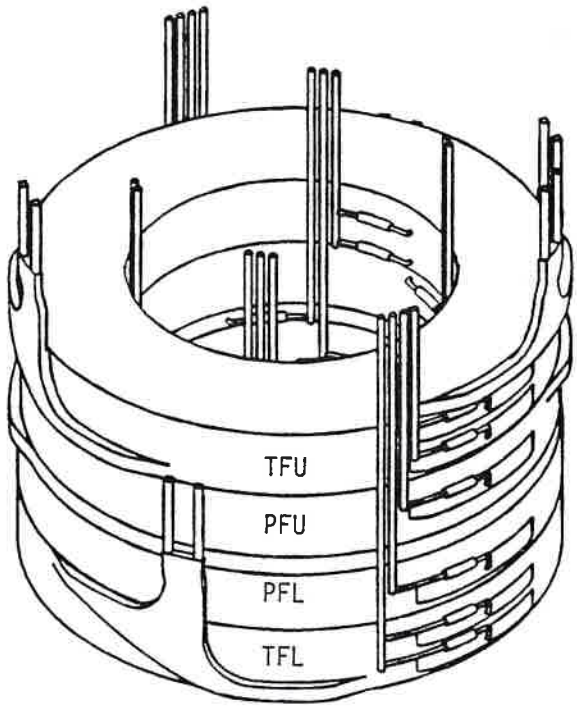

Figure 12 View of the NET model coil stack in the configuration to be tested in the TOSKA facility at KfK (Kernforschungszentrum Karlsruhe, FRG)

modules. In this scenario a coil quench has to be expected as quite a common event during the test, and the test facility must be designed and equipped to be able to respond to the normal zone development quickly enough to prevent any damage to the test facility and to the module itself with regard to mechanical, electrical and hydraulic integrity. For the design of the coil dump circuitry and of the vent lines in the helium supply a detailed quench analysis of the coil is necessary.

Inputs for the analyses

The main inputs for the analyses are reported in *Table 2*. The coil analysed is the upper module of the two PF model coils (inner coils), called here PFU, which will be wound using a braid-based conductor. We assumed an RRR of 100, following the specifications of the manufacturer, and a total operating strain in the strand of −0.6%. The PFU module itself is formed by four double pancakes, with a flow path length (single pancake) of about 130 m. A typical friction factor correlation for a cable-in-conduit conductor was used (5 times higher f than for a smooth tube of the same hydraulic diameter). Assuming a pressure drop of 0.5 bar in one flow path, the mass flow rate was computed according to the specified inlet conditions (about 10 g s^{-1}). In reality a slightly higher value was used (12 g s^{-1}) without any effect on the quench evolution. This was only related to the numerical aspects of the establishment of the initial conditions through pressure boundary conditions. In all cases the boundary condition for the helium flow was taken to be a constant pressure reservoir (large volume).

Table 2 Conductor and coil data used for the analyses presented

Non-copper area	(cm^2)	1.70
Copper area	(cm^2)	2.55
Helium area	(cm^2)	3.39
Steel area	(cm^2)	9.75
Insulation area	(cm^2)	1.31
Wetted perimeter conductor	(m)	1.47
Wetted perimeter jacket	(m)	0.06
Contact perimeter conductor – jacket	(m)	0.06
Hydraulic diameter	(mm)	0.88
Copper RRR	(–)	100
Operating strain	(%)	−0.6
Winding type		Double pancakes One-in-hand
Flow path length	(m)	130
Inlet pressure	(bar)	6.0
Inlet temperature	(K)	4.5
Steady state pressure drop	(bar)	0.5
Steady state mass flow rate	(g s^{-1})	12
Steady state flow velocity	(m s^{-1})	0.25

Quench followed by a coil dump

The operating current was assumed to be 40 kA in the module analysed, while it was set to 54 kA in the other three modules. With these currents a field of about 12.5 T was attained in the inner bore of the PFU module. The magnetic field distribution was taken in all pancakes to be equal to the that computed in the central pancake of the module. A matrix of influence coefficients was computed, giving the magnetic field in one turn for a unit current in one of the modules. The current in the PFU module was dumped with a 20 s decay time constant after a 0.5 s detection and switching delay, while it was assumed that the current in the other modules remained constant at the initial value (54 kA). Given the instantaneous value of the currents in the modules and the influence matrix above, it was possible to compute the field in the whole module as a function of position and time.

The quench was initiated by an energy pulse of 5000 mJ cm^{-3} over a length of 2 m in the middle of the

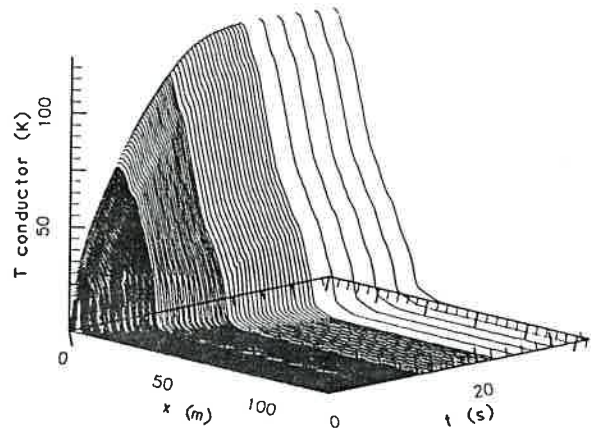

Figure 13 Temperature distribution in the conductor as a function of space and time in the pancake 4 of PFU (initially quenched) during a quench followed by a dump (τ_d = 0.5 s; τ = 20 s)

first turn of pancake 4, and the calculation was performed up to a time of 35 s, when the current has decreased to less than 20% of the initial value (and the Joule heating is less than 5% of the peak value). *Figure 13* reports the temperature distribution in the conductor of the central pancake of the module (initially quenched). While the temperature of the helium closely follows that of the conductor, due to the excellent thermal contact, that of the jacket is well below, up to 25 K lower at 10 s. As time advances, the Joule heat production decreases and with it also the temperature gradients are reduced. At 30 s the difference in temperature between conductor and jacket is below 10 K. The maximum absolute temperature in the conductor is computed at the inlet of pancake 4, and is 125 K. This is considerably below the maximum allowed 150 K. Finally, *Figure 14* shows how the quench spreads on the adjacent pancake of the module after 12 s.

The maximum pressure in the quenched pancake slightly exceeds 27 bar, although most of this peak is due to the high initial heating pulse. In reality this does not represent a significant design case as regards the pressure peaking because the initial normal length is very short. As shown in *Figure 15*, the normal zone is initially only 6 m long, and grows significantly in the initial stage of the dump, when the Joule heating is high. The average speed during the first 10 s of the transient is 2 m s^{-1}, which is very close to the helium expulsion velocity from the normal zone. The maximum normal length (about 45 m) is reached at the end of the calculations, when the propagation speed has decreased to 0.6 m s^{-1}.

The helium flow reversal at inlet reaches a peak of 0.5 kg s^{-1} at the pulse start. The total mass expelled from the pancake is approximately 1.9 kg in 35 s, of which about 0.7 kg are expelled from the pancake inlet, at high temperature (up to about 125 K), and 1.2 kg are expelled from the coil outlet, at low temperature (from 4.5 to 4.7 K). The reason for the lack of symmetry between inlet and outlet during the transient is in the location of the initial normal zone, in the first turn. The helium is quickly expelled from the coil inlet and a zone of low density/high temperature is formed in the first turns. On the other hand the helium close to the coil outlet is still cold and at high density. As the quench proceeds, the expulsion becomes more symmetric because the location of the maximum pressure (flow reversal) moves downstream. The helium velocity at inlet and outlet tends to similar values, but the mass flow is much higher at the outlet by virtue of the higher density in this region of the coil.

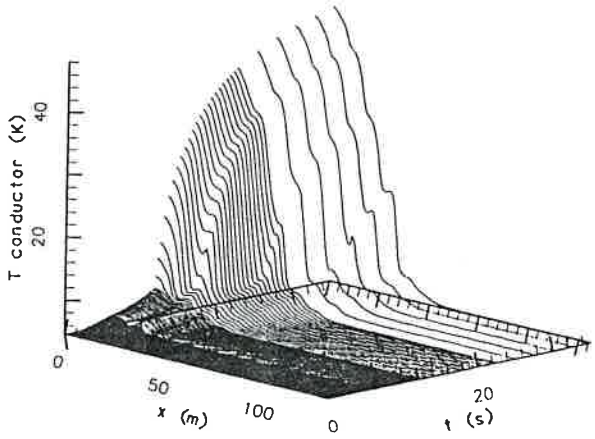

Figure 14 Temperature distribution in the conductor as a function of space and time in the pancake 5 of PFU (adjacent to the initially quenched one) during a quench followed by a dump (τ_d = 0.5 s; τ = 20 s)

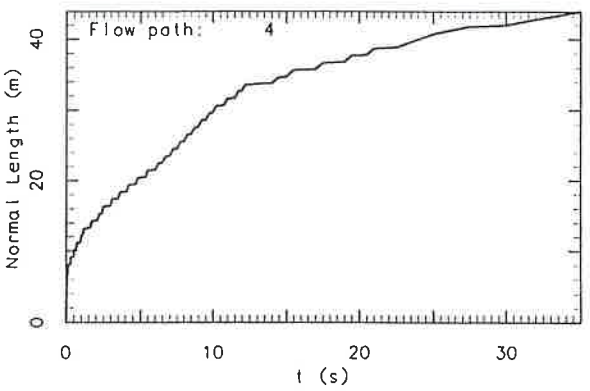

Figure 15 Normal zone evolution in the pancake 4 of PFU (initially quenched) during a quench followed by a dump (τ_d = 0.5 s; τ = 20 s)

Quench with a coil module shorted

The capabilities implemented in the 3-D quench analysis code allow any electrical network connection for the coil under analysis to be specified. In order to investigate the self-protecting capabilities of one coil module it was assumed that the modules were connected in series and that in addition on the terminals of the module PFU a short circuit with zero resistance was present. In this condition the module can reach the maximum current conceivably possible (by induction) without any possibility of external dump of the energy. A quench was initiated in the first turn or the fourth pancake of the module PFU with the stack running at 54 kA (at the predicted critical line). As a consequence a fast discharge was triggered, inserting a 0.4 Ω resistor in series to the stack.

A schematic view of the circuit analysed is given in *Figure 16*. Thc coil inductances were taken from

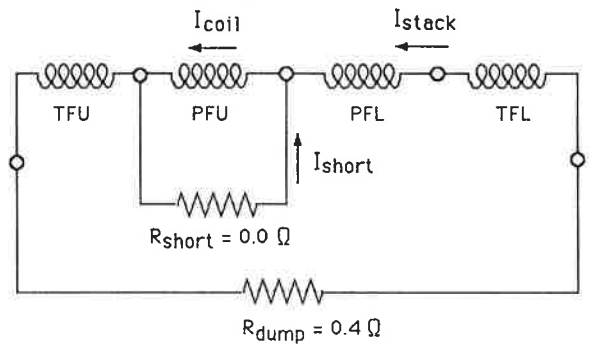

Figure 16 Schematic view of the circuit used for the calculation of the coil quench with one module shorted

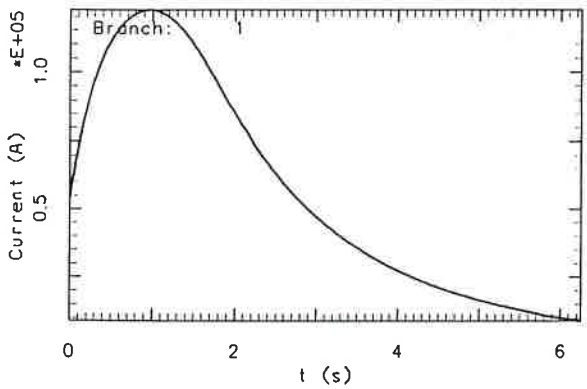

Figure 17 Evolution of the current in the shorted module

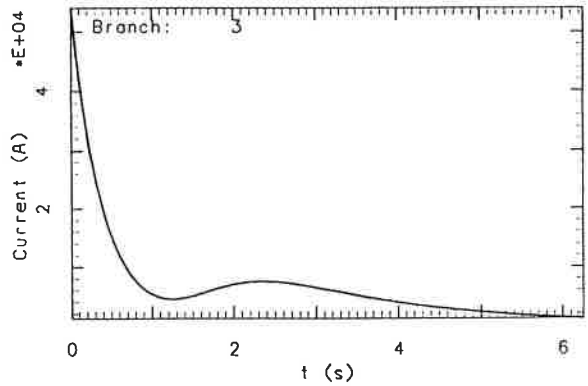

Figure 19 Evolution of the current in the coil stack

Reference 1. The magnetic field was computed as in the analysis presented in the previous section assuming a piecewise constant distribution along the length, with discontinuous field values at the transition from one turn to the next.

The dump of the coil stack induces an over current in the shorted coil loop. The magnetic field distribution changes substantially but, in order to maintain the flux linked, the peak field in the module remains nearly constant during the first second of the dump. The main effect of the current rise is that the superconductor reaches the critical current condition at the inner bore already in the first tenths of a second of the dump, causing a quick quench of all pancakes. As a consequence a resistance develops in the module and the current is dumped as the magnetic energy transferred by inductive coupling is dissipated by the Joule heating. In *Figure 17* the profile of the current in the shorted module is shown. After a sharp increase up to 122 kA, the coil is dumped to less than 8 kA in 6 s. The maximum temperature, as shown in *Figure 18*, is reached in the cable at the end of the transient simulation and is around 400 K. At this time the Joule heating is less than 1% of its peak value.

In the other coils of the stack the current has the behaviour reported in *Figure 19*, where, after the initial decrease due to the insertion of the dump resistor, the current rises again as a consequence of the fast self-dump of the shorted module. Finally, *Figure 20* gives the energy dissipated in the shorted module as a function of time. The maximum value is about 380 MJ, roughly 50% of the initial magnetic energy in the stack

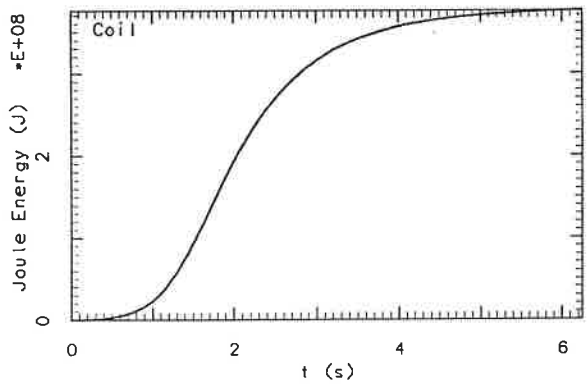

Figure 20 Energy dissipated by the Joule heating in the shorted module

The pressure reaches the maximum value of 250 bar at 2 s after the quench start. The helium expulsion reaches peaks of 1.25 kg s^{-1} at the coil inlet and 1.65 kg s^{-1} at the coil outlet also after 2 s. In total about 2 kg of helium are expelled from the inlet, and 3 kg from the outlet. As the initial mass of helium in the pancake is 6.2 kg, nearly all the helium is blown out of the module within 6 s.

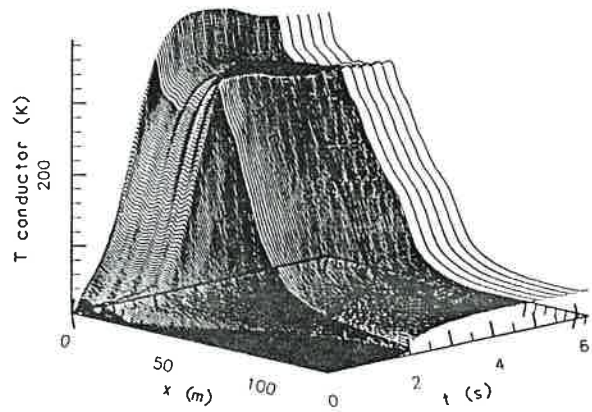

Figure 18 Temperature distribution in the conductor as a function of space and time in the pancake 4 of PFU during a quench with one module shorted

Conclusion

We have shown applications of the 3-D quench propagation model to the simulation of experiments and to the verification of a coil design. The comparison of simulation results and experimental data is favourable, and indicates that the model is complete and reliable. The range of validity is extremely wide, covering the full time scale of the thermal events in a superconductor, from stability to safety relevant transients. These results were achieved at reasonable CPU expenses and model complexity, thus allowing the analysis of a full magnetic system consisting of several coils. These characteristics

are the main features of the model proposed. We believe that they will allow an extensive use of this tool in the design of large size, force-flow cooled superconducting magnets.

References

1 **Bottura, L. and Zienkiewicz, O.C.** Quench analysis of large superconducting magnets. Part I: model description *Cryogenics* (1992) **32** 659–667

2 **Benkowtisch, J.** Untersuchung von örtlich und zeitlich veränderlichen Energieeinkopplungen in das Kühlsystem eines durch flüssiges Helium zwangsgekühlten supraleitenden Magneten, KfK Report 2813, Karlsruhe (1979)

3 **Benkowitsch, J. and Krafft, G.** Numerical analysis of heat-induced transients in forced flow helium cooling systems *Cryogenics* (1980) **20** 209–215

4 **Miller, J.R, Dresner, L., Lue, J.W., Shen, S.S. and Yeh, H.T.** Pressure rise during the quench of superconducting magnet using internally cooled conductors *Proc ICEC-8*, Genoa, Italy, IPC Science and Technology Press, Guildford, UK (1980) 321–329

5 **Lue, J.W., Miller, J.R., Dresner, L. and Shen, S.S.** Simulation of the quenching of an internally cooled superconducting magnet *Proc ICEC-9*, Kobe, Japan, Butterworths, London, UK (1982) 814–818

6 **Lue, J.W., Miller, J.R. and Lottin, J.C.** Pressure drop measurement on forced flow cable conductors *IEEE Trans Magn* (1983) **15** 53–55

7 **Hooper, R.J.** Friction factor correlations for cable-in-conduit conductors *Memo FEDC-M-84-E/M-016* Fusion Engineering Design Center, ORNL (1984)

8 **Wong, R.L.** Program CICC, flow and heat transfer in cable in conduit conductors – equations and verification, *LLNL Int Rep* UCID-21733 (1989)

9 **Beard, D.S., Klose, W., Shimamoto, S. and Vécsey, G.** Eds, The IAEA large coil task, special issue of *Fusion Eng Des* (1988) **7**

10 **Nöther, G, Gauss, S., Mauser, W., Siewerdt, L., Verbricht, A. and Wüchner, F.** Quench detection system of the EURATOM coil for the Large Coil Task *Cryogenics* (1989) **29** 1148–1153

11 **Annandale, R., Bottura, L., Mitchell, N., Perrella, M. and Salpietro, E.** Model coil design for verification of the coil/conductor concept for the NET coils *Proc 16th Symp Fusion Technol*, North-Holland, London (1991) 1716–1720